nomena of this kind are to be found in many, if not most, physiological signaling systems.

REFERENCES AND NOTES

1. F. E. Bloom, *FASEB J.* **2**, 32 (1988); R. A. Nicoll, *Science* **241**, 545 (1988); I. Kupfermann, *Physiol. Rev.* **71**, 683 (1991).
2. B. Hille, *Neuron* **9**, 187 (1992).
3. *Trends Biochem. Sci.* **17** (no. 10) (1992); H. R. Bourne and R. Nicoll, *Cell* **72**/*Neuron* **10** (suppl.), 65 (1993); F. L. Bygrave and H. R. Roberts, *FASEB J.* **9**, 1297 (1995); R. Iyengar, *Science* **271**, 461 (1996).
4. J. L. Cohen, K. R. Weiss, I. Kupfermann, *J. Neurophysiol.* **41**, 157 (1978).
5. E. C. Cropper, I. Kupfermann, K. R. Weiss, *Brain Res.* **522**, 176 (1990); P. J. Church and P. E. Lloyd, *J. Neurophysiol.* **72**, 1794 (1994).
6. K. R. Weiss, J. L. Cohen, I. Kupfermann, *J. Neurophysiol.* **41**, 181 (1978).
7. E. C. Cropper *et al.*, *Proc. Natl. Acad. Sci. U.S.A.* **85**, 6177 (1988).
8. E. C. Cropper *et al.*, *J. Neurophysiol.* **72**, 2181 (1994).
9. P. E. Lloyd, I. Kupfermann, K. R. Weiss, *Proc. Natl. Acad. Sci. U.S.A.* **81**, 2934 (1984).
10. E. C. Cropper *et al.*, *ibid.* **84**, 3486 (1987).
11. E. C. Cropper *et al.*, *ibid.*, p. 5483; E. C. Cropper *et al.*, *Peptides* **12**, 683 (1991).
12. M. D. Whim and P. E. Lloyd, *J. Neurosci.* **10**, 3313 (1990).
13. ———, *Proc. Natl. Acad. Sci. U.S.A.* **86**, 9034 (1989).
14. E. C. Cropper *et al.*, *ibid.* **87**, 933 (1990).
15. V. Brezina *et al.*, *J. Neurophysiol.* **74**, 54 (1995).
16. K. R. Weiss *et al.*, *J. Physiol. (Paris)* **87**, 141 (1993).
17. For most modulators in the ARC-muscle system, the available evidence suggests that the effects on contractions can be fully explained by direct action on the muscle fibers, through the pathways in Fig. 1A only [(*15*, *18*, *19*); V. Brezina and K. R. Weiss, *Soc. Neurosci. Abstr.* **19**, 1262 (1993)]. This holds for the SCPs and MMs, as well as the serotonin and FMRF amide–related peptide (FRF) effects in Fig. 2A. Indirect modulation of contractions through changes in transmitter release from the motor neurons—for example, by the buccalins (*7*, *16*)—is not considered here.
18. V. Brezina, C. G. Evans, K. R. Weiss, *J. Neurosci.* **14**, 4393 (1994).
19. ———, *ibid.*, p. 4412.
20. W. C. Probst *et al.*, *Proc. Natl. Acad. Sci. U.S.A.* **91**, 8487 (1994).
21. K. R. Weiss *et al.*, *J. Neurophysiol.* **42**, 791 (1979).
22. S. L. Hooper *et al.*, *Brain Res.* **657**, 337 (1994); S. L. Hooper *et al.*, *Neurosci. Lett.* **179**, 167 (1994).
23. It is likely that B16 co-releases at least nine MMs, MM_A through MM_I (*15*), which act identically in most respects but differ in their ability to activate the K current (*15*, *19*). MM_B and MM_C are not much more effective than the SCPs. However, the other seven MMs activate large K currents, and the most effective of all, MM_A, is overrepresented in the likely released mixture. Thus, the overall effect of MM release from B16 is activation of a large K current as with MM_A alone (*15*). In our experiments here, we therefore apply just MM_A (except in Fig. 3C). Similarly, B15 co-releases SCP_A and SCP_B, which act identically in all respects [(*10*); P. E. Lloyd, *Trends Neurosci.* **9**, 428 (1986)]; we apply just SCP_B.
24. Strictly, the convergence on cAMP is not equal: SCPs can elevate cAMP much higher than MMs can (*9*, *18*, *22*). However, what matters for our purposes here is that the downstream effects of the SCPs and MMs on the Ca current (*18*) (Fig. 3A) and the relaxation rate (Fig. 3C) are equal, probably because only relatively small increases in cAMP are important: for example, they suffice to enhance the Ca current maximally (*18*).
25. In addition to somewhat different experimental protocols (*29*), major variability in this work is due to differences between animals and especially between batches of animals used in different seasons or years. Differences between batches can be much larger than those within each batch. This can be a serious problem in a study such as this that correlates a variety of data sets. As a result, for instance, we cannot be sure that the deviations of the experimental data in Fig. 4 from the model predictions are not simply the result of somewhat different responses of the animals used in the experiments and those used to obtain the data on which the model was based. This provides one justification for keeping the modeling simple and focused only on major features.
26. I. Kupfermann *et al.*, in *Neurons, Networks, and Motor Behavior*, P. S. G. Stein *et al.*, Eds. (MIT Press, Cambridge, MA, in press).
27. A. J. Susswein, K. R. Weiss, I. Kupfermann, *J. Comp. Physiol. A* **123**, 31 (1978).
28. We obtained these estimates by comparing the effects of B15 and B16 stimulation at physiological frequencies and the effects of known concentrations of exogenous SCP and MM [on, for example, cAMP and active protein kinase A (PKA) concentrations in the muscle (*22*)]. With more intense stimulation, the concentration of SCP released from B15 may reach as high as 10^{-5} M (*13*).
29. The contraction measurements are from figures in (*6–9*, *11*, *15*), older unpublished experiments, and experiments done specifically for this report (for example, Fig. 1B): SCP_A and SCP_B, 117 measurements from 40 preparations; MM_A, 20 from 12; MM_B, 47 from 10; MM_C through MM_I, 66 from 28; serotonin, 2 from 2; and FRF_A through FRF_C, 15 from 6. The older experiments were all done basically as in Fig. 1B but with occasional variations [for example, stimulation of B15 rather than B16, shorter interburst intervals (but not less than 10 s), or shorter modulator exposure before measurement (but not less than 2.5 min)], which may account for some of the variability. The Ca and K current values are mean values (n = 3 to 7) pooled from dose-response plots in (*8*, *15*, *18*, *19*); where necessary, linear interpolation was used, along with the fact that SCP_A and SCP_B act identically (*23*), as do FRF_A through FRF_C (*8*) and, on the Ca current, MM_A through MM_I (*15*, *18*) (Fig. 3, A and B, shows a subset of the same data). The FRFs are assumed not to modulate the Ca current (*8*). For normalization of the data, see (*30*).
30. Contraction size is always expressed as a percentage of control size (control = 100%, no contraction = 0%), Ca current enhancement is expressed as the percentage increase over control current amplitude (control = 0%), and K current activation is expressed as a percentage of the current activated by saturating MM_A, which is the largest and occludes all others (*8*, *15*, *19*) (no current = 0%, saturating MM_A = 100%) (desensitization of the K current response is ignored). Relaxation rate is expressed as a percentage of the range within each experiment (control = 0%, fastest rate induced by high SCP or MM = 100%). In Fig. 3C, SCP and MM were tested in separate experiments; however, the following information shows that 100% represents essentially the same absolute maximal effect for both. In four of the experiments with SCP_B and four matched experiments with MM_B, SCP_B increased the relaxation rate from 0.87 ± 0.05 s^{-1} (= 0%) to 3.99 ± 0.90 s^{-1} (= 100%), and MM_B increased it from 1.06 ± 0.09 to 4.01 ± 0.61 s^{-1} (mean ± SEM). Moreover, maximal SCP and MM effects were mutually occlusive ("SCP + MM_B").
31. V. Brezina and K. R. Weiss, *J. Neurophysiol.* **73**, 993 (1995); *Biophys. J.* **68**, A277 (1995).
32. Quantification of the vertical scatter of the points in Fig. 2A from the surface in Fig. 2B. The mean deviation (experimental − model) and the standard deviation, respectively (in percent): all points, 8.3 and 6.4; SCP_A and SCP_B, −13.5 and 12.0; MM_A, 66.0 and 21.0; MM_B, 33.3 and 15.8; MM_C through MM_I, 7.8 and 5.0; and FRF_A through FRF_C, 8.2 and 6.1 (too few points were available for serotonin). Thus, the points for each modulator lie reasonably evenly above and below and not too far from the surface, except for MM_A and MM_B, which lie somewhat more above the surface.

33. We thank E. C. Cropper and B. Bank for the unpublished data included in Fig. 2A, and E. C. Cropper, M. L. Scott, C. Erxleben, and I. Kupfermann for comments on the manuscript. This work was funded by NIH grants MH36730, GM320099 (K.R.W.), and K21 MH00987 (V.B.) and the Whitehall Foundation (V.B.).

5 April 1996; accepted 30 May 1996

Organization of Diphtheria Toxin T Domain in Bilayers: A Site-Directed Spin Labeling Study

Kyoung Joon Oh, Hangjun Zhan,* Can Cui, Kálmán Hideg, R. John Collier,† Wayne L. Hubbell†

The diphtheria toxin transmembrane (T) domain was spin-labeled at consecutive residues in a helical segment, TH9. After binding of the T domain to membranes at low pH, the nitroxide side chains generated by spin labeling were measured with respect to their frequency of collision with polar and nonpolar reagents. The data showed that the helical structure of TH9 in solution is conserved, with one face exposed to water and the other to the hydrophobic interior of the bilayer. Measurement of the depth of the nitroxide side chains from the membrane surfaces revealed an incremental change of about 5 angstroms per turn, which is consistent with a transmembrane orientation of an α helix. These results indicate that the helix forms the lining of a transmembrane water-filled channel.

Diphtheria toxin (DT) (*1*) belongs to a large class of toxic proteins that act by enzymatically modifying cytosolic substrates within eukaryotic cells (*2*). The process by which the catalytic moiety is transferred across a membrane lipid bilayer into the cytosol is not understood for any such toxin. For DT, translocation occurs only after the toxin has bound to its receptor at the cell surface and has been delivered by receptor-mediated endocytosis to the endosomal compartment (*3*). Under the influence of the low pH within that compartment, the toxin undergoes a conformational rearrangement that causes its T domain to insert into the endosomal membrane (*4*). This insertion event is known to induce the toxin's catalytic domain to cross the membrane to the cytosolic compartment (*5*), where it catalyzes the adenosine diphos-

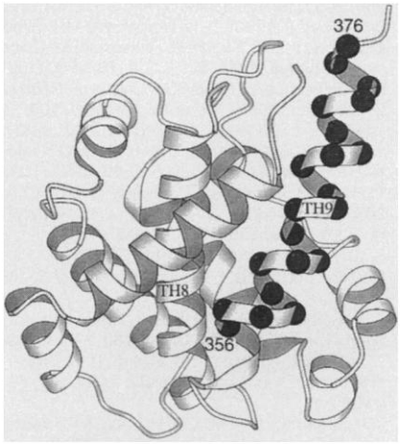

Fig. 1. Structure of the T domain (residues 202 to 378) of DT. The locations of 21 residues selected for mutation to cysteine and attachment of spin probes are indicated as solid spheres. Mutants of the isolated T domain were prepared as described (*15*). The numbering of the mutant residues is that of the native DT. This Molscript representation (*23*) was generated from the coordinates of DT provided by Bennett and Eisenberg (*8*).

phate ribosylation of elongation factor–2, causing inhibition of protein synthesis and cell death (6).

The T domain (Fig. 1), which is situated between the toxin's NH_2-terminal catalytic and COOH-terminal receptor-binding domains, is composed of nine α helices (*7*, *8*). Two long hydrophobic helices, TH8 and TH9, form a helical hairpin in the core of the T domain and are covered by two other "layers" of helices (9). The holotoxin or the isolated T domain forms voltage-dependent channels in planar bilayers under low-pH conditions (pH ~5) (*10*), and a toxin subfragment containing TH8 and TH9 as the only components of the T domain is sufficient for channel formation (*11*). Chemical modification studies indicate that the TH8-TH9 interhelical loop is located on the trans surface of the bilayer in the open channel state (*12*). Thus, it has been postulated that the DT channel is formed by the insertion of the TH8-TH9 helical hairpin into the membrane (*7*, 9, *12*). However, direct evidence that this motif retains its helical structure in the membrane is lacking, and the structure of the conducting unit is unknown.

K. J. Oh and W. L. Hubbell, Jules Stein Eye Institute and Department of Chemistry and Biochemistry, University of California, Los Angeles, CA 90095–7008, USA.
H. Zhan, C. Cui, R. J. Collier, Department of Microbiology and Molecular Genetics, Harvard Medical School, 200 Longwood Avenue, Boston, MA 02115, USA.
K. Hideg, Central Research Laboratory, Chemistry, University of Pécs, H-7643 Pécs, Hungary.
*Present address: Arris Pharmaceutical Corporation, 385 Oyster Point Boulevard, Suite 3, South San Francisco, CA 94080, USA.
†To whom correspondence should be addressed.

Fig. 2. Reaction of spin label to generate nitroxide side chain R1.

Site-directed spin labeling (SDSL) offers a promising approach for resolving secondary structure and tertiary interactions in proteins (*13*). To explore the structure of the membrane-bound state in the isolated T domain, we prepared 21 single-cysteine substitution mutants (Fig. 1) and modified each with a methanethiosulfonate spin label (MTSSL) to generate a nitroxide side chain, designated R1 (Fig. 2). The electron paramagnetic resonance (EPR) spectra of the spin-labeled mutants bound to phospholipid vesicles (*14*, *15*) are shown in Fig. 3.

To determine the topographical locations of the R1 side chains in the membrane, we used power saturation techniques to assess the collision frequencies of the nitroxides with polar and nonpolar paramagnetic reagents [Ni(II)-ethylenediaminediacetate complex (NiEDDA) and O_2, respectively] (*16*). These frequencies are expressed in terms of the proportional accessibility parameter Π (*17*). For a membrane-bound protein, a nitroxide immersed in the bilayer has a high accessibility to O_2 but a low accessibility to NiEDDA, and the reverse is true for a nitroxide in water, because of the differential solubility of the reagents in the two phases. A plot of $\Pi(O_2)$ and Π(NiEDDA) as a function of amino acid number for the membrane-bound T domain (Fig. 4A) shows that the collision frequencies for both reagents display a periodicity in sequence position, with an average period of 3.5 residues, approximately that of an α helix. Similar results were reported earlier for collision frequencies with O_2 in the bacteriorhodopsin E helix (*18*). However, the oscillatory behaviors for $\Pi(O_2)$ and Π(NiEDDA) are 180° out of phase with each other (Fig. 4A). This pattern indicates a helical structure throughout the sequence, with one face solvated by water and the other by the hydrophobic interior of the bilayer.

The maxima in $\Pi(O_2)$ occur at residues 357, 360, 363, 367, and 371; the maxima in Π(NiEDDA) occur at residues 356, 359, 362, 366, 369, and 372 (Fig. 4A). These maxima represent sites on the outer surface of the helix that face the bilayer and water, respectively. This interpretation is supported by the finding that the nitroxide mobilities at these sites, reflected in the spectral line shapes, are similar to those observed on the outer surfaces of helices in bacteriorhodopsin (*16*) and T4 lysozyme (*19*), respectively. Moreover, the residues facing the bilayer are hydrophobic (originally buried within the hydrophobic interior or at tertiary contact sites in the T domain in solution), whereas the residues facing the aqueous phase are polar (either exposed or near tertiary contact sites in the solution structure). A helical wheel representation of the sequence studied is shown in Fig. 4B.

The accessibility data are consistent with either of the two general models shown in Fig. 4D for the interaction of the TH8-TH9 helical hairpin with membranes. For the surface-adsorbed helix (model 1), the most deeply buried residues facing the bilayer interior are all at the same depth in the membrane, whereas in the transmembrane channel (model 2), successive residues on the helix surface facing the bilayer are located at increasing depths, reaching a maximum at the membrane center. Because gradients of O_2 and NiEDDA exist in the bilayer at equilibrium, collision frequencies are depth dependent, and the quantity $\Phi = \ln[\Pi(O_2)/\Pi(\text{NiEDDA})]$ is a linear function of depth for a nitroxide in the membrane (*16*). Calibration of Φ using spin-labeled phospholipids with nitroxides at known depths in

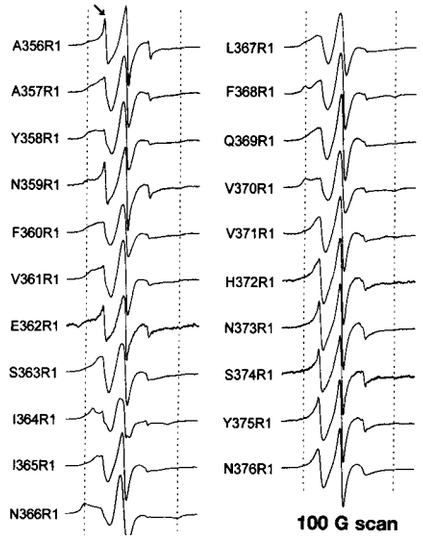

Fig. 3. EPR spectra of spin-labeled T domain mutants in the presence of phospholipid vesicles at pH 4.6. Spin-labeled T domain mutants (*24*, *25*) bound to vesicles containing POPG-POPC (*14*) were prepared as described (*15*). The vertical dashed lines mark the locations of outer hyperfine extrema. The sharp features in some spectra are the result of a small amount of unattached spin label (the arrow indicates one example).

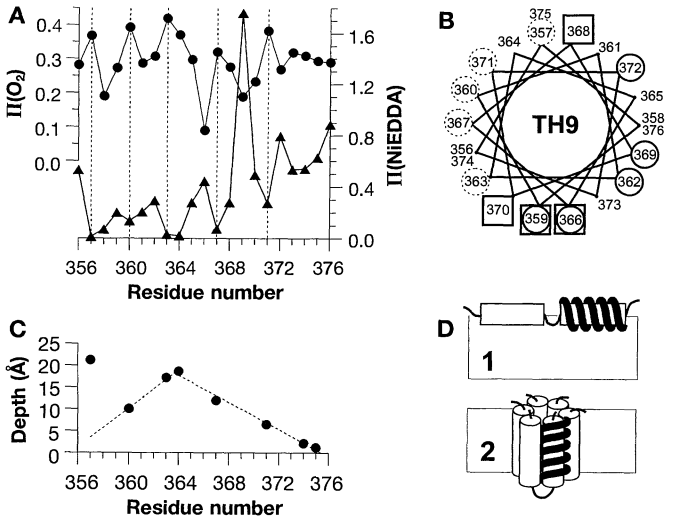

Fig. 4. (**A**) Accessibility parameters $\Pi(O_2)$ (●) and Π(NiEDDA) (▲) versus residue number (*26*). (**B**) Helical wheel showing locations of the spin-labeled residues. Dashed and solid circles denote residues at the maxima of $\Pi(O_2)$ and Π(NiEDDA), respectively. Squares indicate sites of immobilized residues. (**C**) Immersion depth of R1 chains versus residue number (*20*). (**D**) Two schematic models for the organization of the TH8-TH9 helical hairpin in a membrane. In model 1, helices are adsorbed on the surface of the membrane. In model 2, a water-filled channel formed from an association of helical hairpins is inserted across the membrane. Three associated hairpins are the minimum required for channel formation. The heavy lines schematically indicate the regions scanned in TH9.

the bilayer allows calculation of the depth of the R1 side chain from the membrane-solution interface (*20*). For nitroxide side chains in a protein, this analysis is valid only for sites facing the bilayer interior (*16*).

For the residues located on the surface of the helix facing the hydrophobic interior of the bilayer, the data (as calculated from Φ) reveal that successive residues vary in depth by increments of ~5 Å, with residue 364 near the center of the bilayer (Fig. 4C); this finding is consistent with a transmembrane orientation of the α helix. Only residue 357 lies at a depth greater than that predicted from the simple model 2, which suggests an irregularity in the structure near the NH_2-terminus of the helix. In the crystal structure of DT, the first turn in the NH_2-terminus of TH9 (residues 356 to 359) is also irregular (8) (Fig. 1). Collectively, these data argue strongly for the existence of a water-filled channel lined by helix TH9 of the T domain of DT.

The maxima in Π(NiEDDA) increase regularly from the NH_2-terminal to the COOH-terminal sites in the putative transmembrane helix. This observation implies that the concentration-diffusion product of NiEDDA is attenuated along the length of the channel. Such an effect may arise from a constriction near the NH_2-terminal region, which in turn may be related to the voltage gate of the channel.

Further support for a transmembrane channel lined by TH9 comes from an analysis of the mobility of the nitroxide side chains. The majority of the EPR spectra are complex, reflecting multiple components. However, several of these spectra have unique features that are readily identified. For example, residues 359, 366, 368, and 370 have spectral components with well-resolved outer hyperfine extrema in the range of 66 to 70 G; this feature defines an immobilized nitroxide (Fig. 3). Such sites provide a map of tertiary or quaternary contact surfaces in the TH9 helix. These surfaces lie between the water- and bilayer-exposed surfaces of the helix (Fig. 4B), as would be expected in a helical bundle arrangement of the type shown in Fig. 4D. Although similar nitroxide-scanning experiments must be carried out in the remainder of the T domain to determine the complete structure, the above data offer strong support for a transmembrane organization in which the TH9 helix lines a water-filled channel.

Our results extend earlier SDSL studies on membrane proteins (*13*) and reveal periodic out-of-phase accessibilities to polar and nonpolar reagents for asymmetrically solvated helices. In addition, the experiments demonstrate that nitroxide-scanning SDSL can provide sequence-specific secondary structure data. This method should complement current techniques for investigating the structure of membrane-associated peptides and proteins, including those involved in translocation processes (*21*).

REFERENCES AND NOTES

1. R. J. Collier, *Bacteriol. Rev.* **39**, 54 (1975); A. M. Pappenheimer Jr., *Annu. Rev. Biochem.* **46**, 69 (1977); L. Greenfield *et al.*, *Proc. Natl. Acad. Sci. U.S.A.* **80**, 6853 (1983).
2. J. Moss, B. Iglewski, M. Vaughan, A. T. Tu, Eds., *Bacterial Toxins and Virulence Factors in Disease: Handbook of Natural Toxins* (Dekker, New York, 1995), vol. 8.
3. R. E. Morris, A. S. Gerstein, P. F. Bonventre, C. B. Saelinger, *Infect. Immun.* **50**, 721 (1985); J. G. Naglich, J. E. Metherall, D. W. Russell, L. Eidels, *Cell* **69**, 1051 (1992).
4. E. London, *Biochim. Biophys. Acta* **1113**, 25 (1992); D. Tortorella, D. Sesardic, C. S. Dawes, E. London, *J. Biol. Chem.* **270**, 27446 (1995); V. Cabiaux *et al.*, *Mol. Microbiol.* **11**, 43 (1994); J. O. Moskaug, H. Stenmark, S. Olsnes, *J. Biol. Chem.* **266**, 2652 (1991); K. Sandvig and S. Olsnes, *J. Cell Biol.* **87**, 828 (1980); R. K. Draper and M. I. Simon, *ibid.*, p. 849; B. L. Kagan, A. Finkelstein, M. Colombini, *Proc. Natl. Acad. Sci. U.S.A.* **78**, 4950 (1981).
5. C. Montecucco, E. Papini, G. Schiavo, E. Padovan, O. Rossetto, *FEMS Microbiol. Immunol.* **105**, 101 (1992); I. H. Madshus, A. Wiedlocha, K. Sandvig, *J. Biol. Chem.* **269**, 4648 (1994); D. O. O'Keefe *et al.*, *Proc. Natl. Acad. Sci. U.S.A.* **89**, 6202 (1992).
6. T. Honjo, Y. Nishizuka, O. Hayaishi, *J. Biol. Chem.* **243**, 3553 (1968); B. G. Van Ness, J. B. Howard, J. W. Bodley, *ibid.* **255**, 10717 (1980).
7. S. Choe *et al.*, *Nature* **357**, 216 (1992).
8. M. J. Bennett and D. Eisenberg, *Protein Sci.* **3**, 1464 (1994).
9. J. A. Silverman, J. A. Mindell, A. Finkelstein, W. H. Shen, R. J. Collier, *J. Biol. Chem.* **269**, 22524 (1994).
10. J. A. Mindell, H. Zhan, P. D. Huynh, R. J. Collier, A. Finkelstein, *Proc. Natl. Acad. Sci. U.S.A.* **91**, 5272 (1994).
11. J. A. Silverman, J. A. Mindell, H. Zhan, A. Finkelstein, R. J. Collier, *J. Membr. Biol.* **137**, 17 (1994).
12. J. A. Mindell, J. A. Silverman, R. J. Collier, A. Finkelstein, *ibid.*, p. 29.
13. W. L. Hubbell and C. Altenbach, in *Membrane Protein Structure: Experimental Approaches*, S. White, Ed. (Oxford Univ. Press, London, 1994), pp. 224–248; *Curr. Opin. Struct. Biol.* **4**, 566 (1994).
14. Large unilamellar vesicles containing a molar ratio of 17% 1-palmitoyl-2-oleoyl-*sn*-3-phospho-*rac*(1-glycerol) (POPG) and 83% 1-palmitoyl-2-oleoyl-*sn*-glycero-3-phosphocholine (POPC) were used in this experiment.
15. H. Zhan, K. J. Oh, Y.-K. Shin, W. L. Hubbell, R. J. Collier, *Biochemistry* **34**, 4856 (1995).
16. C. Altenbach, D. A. Greenhalgh, H. G. Khorana, W. L. Hubbell, *Proc. Natl. Acad. Sci. U.S.A.* **91**, 1667 (1994).
17. Z. T. Farahbakhsh, C. Altenbach, W. L. Hubbell, *Photochem. Photobiol.* **56**, 1019 (1992).
18. C. Altenbach, T. Marti, H. G. Khorana, W. L. Hubbell, *Science* **248**, 1088 (1990).
19. H. Mchaourab, M. A. Lietzow, K. Hideg, W. L. Hubbell, *Biochemistry*, in press.
20. The immersion depths of the R1 chains were calculated from values of Φ and a calibration curve [depth (in angstroms) = (4.81Φ + 4.9)]. This calibration curve was obtained with the use of spin-labeled phospholipids with nitroxides at different depths along the hydrocarbon chain (*16*) and *N*-tempoyl palmitamide (*22*) in the host phospholipid vesicles containing POPG-POPC (*14*) at pH 4.6.
21. B. Martoglio, M. W. Hofmann, J. Brunner, B. Dobberstein, *Cell* **81**, 207 (1995).
22. Y.-K. Shin and W. L. Hubbell, *Biophys. J.* **61**, 1443 (1992).
23. P. J. Kraulis, *J. Appl. Crystallogr.* **24**, 946 (1991).
24. To designate mutants with side chain R1 (Fig. 2), we use the notation XYR1, where X is the single-letter code for the original amino acid (A, Ala; E, Glu; F, Phe; H, His; I, Ile; L, Leu; N, Asn; Q, Gln; S, Ser; V, Val; Y, Tyr) and Y is the position of the cysteine substitution.
25. The protein mutants used in this experiment have four additional residues at the NH_2-terminus, Gly-Ser-His-Met. A cysteine substitution mutant at residue 362 contains a $(His)_6$-Gly-Ser-His-Met tail at the NH_2-terminus.
26. Values of $\Pi(O_2)$ and Π(NiEDDA) were measured for the spin-labeled T domain mutants bound to vesicles containing POPG-POPC (lipid/protein molar ratio, 500:1) at pH 4.6, as described (*14*, *15*). The O_2 concentration was that in equilibrium with air, and the concentration of NiEDDA was 200 mM.

27. Supported by NIH grants AI-22021 and AI-22848 (R.J.C.) and EY-05216 (W.L.H.), Hungarian National Research Foundation grant OTKA/T017842 (K.H.), and the Jules Stein Professor Endowment (W.L.H.). We thank M. J. Bennett, C. E. Bell, and D. Eisenberg for providing the coordinates of the refined DT crystal structure, and D. Eisenberg, J. R. Trudell, D. Bok, C. Altenbach, H. Mchaourab, D. Farrens, and R. Langen for reading the manuscript and helpful discussions.

15 April 1996; accepted 13 June 1996